

Alfvén Waves and Turbulence in the Solar Atmosphere and Solar Wind

Andrea Verdini ¹

and

Marco Velli ²

ABSTRACT

We solve the problem of propagation and dissipation of Alfvénic turbulence in a model solar atmosphere consisting of a static photosphere and chromosphere, transition region, and open corona and solar wind, using a phenomenological model for the turbulent dissipation based on wave reflection. We show that most of the dissipation for a given wave-frequency spectrum occurs in the lower corona, and the overall rms amplitude of the fluctuations evolves in a way consistent with observations. The frequency spectrum, for a Kolmogorov-like slope, is not found to change dramatically from the photosphere to the solar wind, however it does preserve signatures of transmission throughout the lower atmospheric layers, namely oscillations in the spectrum at high frequencies reminiscent of the resonances found in the linear case. These may disappear once more realistic couplings for the non-linear terms are introduced, or if time-dependent variability of the lower atmospheric layer is introduced.

Subject headings: MHD – waves – turbulence – Sun: solar wind

1. INTRODUCTION

In situ measurement of magnetic and velocity field fluctuations from Helios and Ulysses have revealed a broad developed spectrum for frequencies ranging from 10^{-4} Hz to 10^{-2} Hz. Typically, a strong correlation between magnetic field and velocity fluctuations in this distance range persists (Mangeney et al. 1991) corresponding to an outwardly propagating spectrum. It is well known that nonlinear terms couple Alfvén waves propagating in opposite

¹Dipartimento di Astronomia e Scienza dello Spazio, Università degli Studi di Firenze, Firenze, Italy

²JPL, California Institute of Technology, Pasadena, California, US.; on leave of absence from the Dipartimento di Astronomia e Scienza dello Spazio, Università degli Studi di Firenze, Italy

directions. Also, the basic nonlinearity in homogeneous MHD in the presence of a majority of one type of waves forces the evolution with time to increase the dominance, preferentially dissipating the minority component in a process called dynamical alignment (Veltri et al. 1980) which is not observed in the solar wind. Therefore the presence of a well-developed spectrum together with a preferred direction of propagation has remained a mystery. The question that naturally arises therefore concerns the drivers for the continuing and anomalous (compared to homogeneous MHD predictions) nonlinear cascade in this outwardly dominant case. Among the possible drivers of a nonlinear cascade in the solar atmosphere are compressible effects, which couple Alfvén waves with slow and fast modes, or couplings due to the strong gradients in the atmosphere. Among the first are phenomena such as parametric decay (Pruneti & Velli 1997; Del Zanna et al. 2001) and wave-steepening (Suzuki & Inutsuka 2005). Gradients transverse to the mean magnetic field directions lead to phase-mixing, i.e. development of small scales in directions perpendicular to that of propagation. Finally, the gradients due to stratification cause wave-reflection, which naturally produces the waves propagating in opposite direction required for the classical incompressible cascade, as first suggested by Velli et al. (1989). Disentangling the role of all of these processes at once would require fully 3D calculations in a realistic atmosphere model, a feat beyond present numerical capabilities. We therefore focus here on the role of wave-reflection, which has been extensively studied in the linear case (Heinemann & Olbert 1980; Leroy 1980; Hollweg 1978 among the first) while less so in the nonlinear one (Matthaeus et al. 1983, 1994).

Some constraints on the frequency spectrum and the energies for the outward and inward propagating components are derived from the observations. The Alfvénic fluctuation power spectrum in the fast solar wind evolves with distance (R) not self-similarly with a power-law dependence on ω with slope -1 and -5/3 at low and high frequencies respectively. The two intervals are separated by a critical frequency (ω_*) which depends on R . Identifying the fluctuations with Alfvén waves it is useful to adopt the Elsässer variables $\mathbf{z}^\pm = \mathbf{u} \mp \text{sign}(B_0)\mathbf{b}/\sqrt{4\pi\rho}$ (corresponding respectively to outward and inward propagating Alfvén waves if the mean magnetic field B_0 is pointing outward from the sun) The energy per unit mass residing in the outward and inward propagating modes ($E^\pm = |\mathbf{z}^\pm|^2$ respectively) both decrease with distance and for $R < 2.5$ AU $E^+ \propto R^{-1.48}$ and $E^- \propto E^{-0.42}$ (Bavassano et al. 2000b). The normalized cross helicity, $\sigma_c = (E^+ - E^-)/(E^+ + E^-)$ which accounts for the imbalance between the outward and inward component, also evolves with distance and it is approximately equal to one in the inner solar wind, it decreases for $R > 0.4$ AU and oscillates around ≈ 0.4 for $R > 2.5$ AU (Bavassano et al. 2000a).

It must be recalled that the observed features can not be explained either by linear

propagation theory (including reflection) or by MHD turbulence separately.

A linear analysis applied to the solar wind case shows that low frequency waves ($\omega < 10^{-5}$ Hz) experience the strongest reflection in the photosphere, chromosphere and corona (Hollweg 1978, 1981; Similon & Zargham 1992). Their flux at the transition region is greatly reduced (even if a considerable power is transmitted to the corona) and in the outer (supersonic) solar wind the radial dependence of σ_c is similar to the observed at higher frequencies (Velli et al. 1991).

On the other hand the high frequency waves (10^{-4} Hz $< \omega < 10^{-2}$ Hz) are almost completely transmitted (even if in the photosphere and chromosphere their reflection is relatively high), both the E^+ and E^- energies decrease faster than the scaling observed and finally $\sigma_c \approx 1$ in the outer solar wind (Velli et al. 1991).

The dynamics of a well developed turbulent state in the expanding solar wind has been studied as well and ordering of the characteristic time scale which should effectively favor the development of a turbulent cascade in planes perpendicular to the direction of wave propagation (along the magnetic field) has been found (Zank et al. 1996; Matthaeus et al. 1998, 1999; Dmitruk et al. 2001a, 2002; Dmitruk & Matthaeus 2003; Oughton et al. 2001, 2004). Numerical models capable of reproducing the observed σ_c profiles in the supersonic part of the solar wind (Zhou & Matthaeus 1989, 1990) or the spectral evolution (Tu et al. 1984; Tu 1988; Velli et al. 1989) necessarily use ad hoc assumption and simplification, and, even if considerable advances have been made, a complete understanding of the solar turbulent spectrum and the solar wind acceleration (Li et al. 1999; Habbal et al. 1995) has not been achieved.

Here, we investigate the combined effect of wave reflection and turbulent dissipation in order to understand the relative importance of linear and nonlinear effects on the overall evolution of the fluctuation amplitudes. Comparison of the numerical results with some observations give some constrains on the fields at the photospheric and coronal level for which data are still missing with implications for numerical models of solar wind acceleration.

In the context of a reflection driven turbulent cascade process another interesting issue concerns the evolution of the turbulent spectrum. If one supposes that the Alfvén waves are injected at the photospheric base at a well defined frequency or with a given correlation time one would expect to find a signature of this characteristic time-scale in the observed spectrum at 1 AU (or in other words, one can ask if discrete modes and turbulence can coexist (Dmitruk et al. 2004)). No injection frequency is observed in the solar wind spectrum so one can ask if both the turbulent evolution and the frequency-dependent transmission properties of the solar atmosphere and wind can efficiently smooth this supposed strong forcing signature.

We integrate numerically the equations for the velocity and magnetic field fluctuations (written in terms of the Elsässer fields) for a stationary model atmosphere with a spherically expanding wind, from the photosphere to one AU for a set of frequency chosen in the range $10^{-6} \text{ Hz} < \omega < 10^{-2} \text{ Hz}$. Each wave is identified via its frequency while a phenomenological nonlinear term is added to the equations in order to account for both turbulent dissipation and frequency coupling.

2. THE MODEL

The equations describing the propagation of Alfvén waves in an inhomogeneous stationary medium can be derived from the Magnetohydrodynamic equations (MHD) under the hypotheses of incompressible adiabatic transverse fluctuations. The velocity (\mathbf{u}) and magnetic field fluctuations (\mathbf{b}) can be combined to form the Elsässer variables $\mathbf{z}^{\pm} = \mathbf{u} \mp \text{sign}(\mathbf{B}_0)\mathbf{b}/\sqrt{4\pi\rho}$ which describe Alfvén waves propagating outward (\mathbf{z}^+) or inward (\mathbf{z}^-). \mathbf{B}_0 stands for the average magnetic field while ρ is the mass density. In terms of these variables the equations for the two fields read:

$$\begin{aligned} \frac{\partial \mathbf{z}^{\pm}}{\partial t} + [(\mathbf{U} \pm \mathbf{V}_a) \cdot \nabla] \mathbf{z}^{\pm} + (\mathbf{z}^{\mp} \cdot \nabla)(\mathbf{U} \mp \mathbf{V}_a) + \\ \pm \frac{1}{2}(\mathbf{z}^{\mp} - \mathbf{z}^{\pm})[\nabla \cdot \mathbf{V}_a \mp \frac{1}{2}(\nabla \cdot \mathbf{U})] = -(\mathbf{z}^{\mp} \cdot \nabla) \mathbf{z}^{\pm}, \end{aligned} \quad (1)$$

where \mathbf{U} is the mean wind speed and the Alfvén speed is $\mathbf{V}_a = \mathbf{B}_0/\sqrt{4\pi\rho}$, co-linearity between magnetic and gravitational field is assumed. On the right hand side we have grouped the nonlinear terms (except the total pressure, which in the limit of incompressible fluctuations can also be written as the product of \mathbf{z}^+ , \mathbf{z}^- and their gradients). In the linear part of the eq. 2 we can recognize a propagation term (II) and two terms accounting for reflection due to the variation of the properties of the medium, one isotropic (IV) while the other (III) involves variations along the fluctuations' polarization.

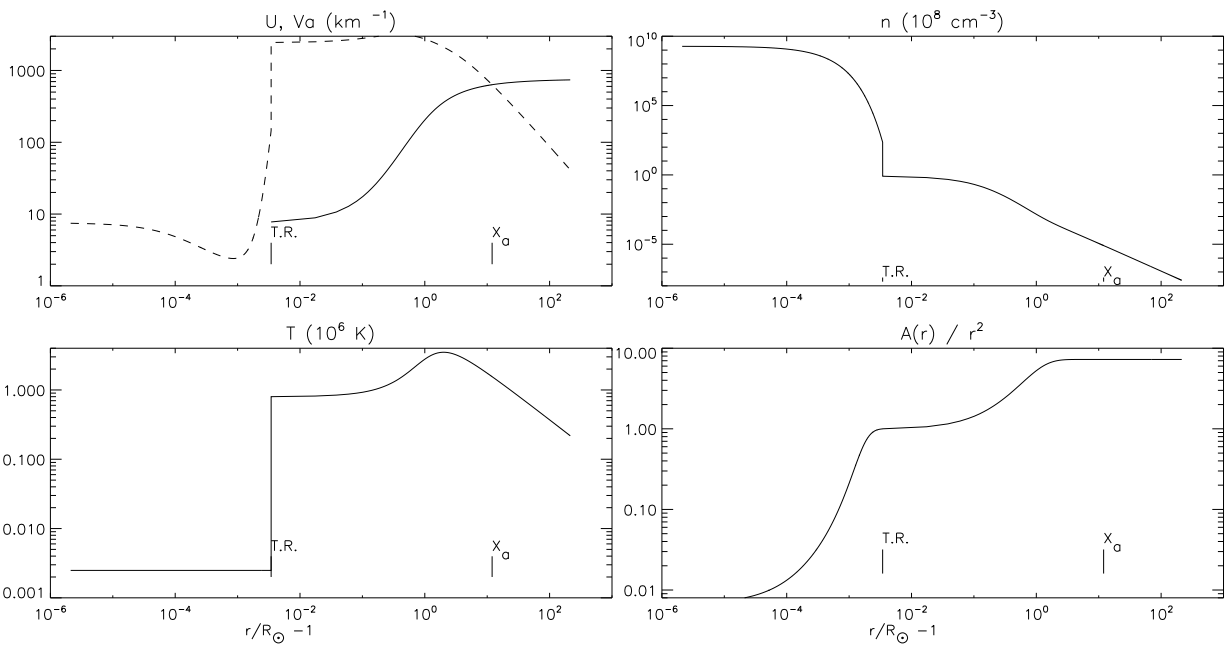


Fig. 1.— From top left, clockwise: wind speed (solid line) and Alfvén speed (dotted line), numerical density, temperature and expansion factor as function of heliocentric distance for the modeled atmosphere.

The chromosphere and the photosphere are modeled as a static layer, 2400 km thick, with the magnetic field organized in flux tube in supra-spherical geometry with constant temperature. The density varies almost exponentially and the magnetic field varies according to the flux tube expansion (A) in order to reproduce the properties of a coronal hole in the quiet Sun (Hollweg et al. 1982). Across the transition region the density falls off by two orders of magnitude, the wind passes from a speed of 0 km s⁻¹ to 8 km s⁻¹ while the magnetic field strength is continuous (about 10 G). The corona also expands supra-spherically and its temperature profile is chosen to fit observations (see fig. 1): it starts at 8×10^5 K at the coronal base, peaks at about 3×10^6 K at $3 R_\odot$ and then falls off with distance as $r^{-0.7}$ (Casalbuoni et al. 1999). The wind speed profile follows from the wind equations with given temperature and flux tube expansion, of the form $A(r) = f(r)r^2$, with f a function which has a maximum close to the coronal base and tends to a finite value at large distances (see Kopp & Holzer 1976, and Munro & Jackson 1977). The same functional form is chosen for the expansion in the static part of the atmosphere but different parameters are selected in order to obtain realistic values for the magnetic field and its continuous variation at the transition region. In the photosphere and chromosphere the profile for Alfvén speed is obtained from the magnetic flux conservation, $B = B_0 A_0 / A(r)$, and the density profile imposed.

Following Dmitruk et al. (2001b) we choose the following model for the nonlinear terms in eq. 2

$$NL_j^\pm = \mathbf{z}^\pm(\omega_j) \frac{|Z^\mp|}{L(r)} \quad (2)$$

where L represents an integral turbulent dissipation length and $|Z^\mp|$ stands for the total amplitude of the Elsässer field integrated over the whole spectrum (Ω) at the point r , hence $|Z^\mp| = \sqrt{\int_\Omega [|\mathbf{z}^\mp(\omega)|^2 / \omega \, d\omega]}$.

This choice overestimates the transfer rate between high-frequency modes, for which the Alfvén effect is important (shebalin et al?). In reality the predominant interaction, as will be seen below, concerns the lowest frequency reflected mode and the full outward propagating spectrum, for which the resonance effects are not important.

The energy distribution among the modes influences the dissipation rate of all the waves coupled. In particular, at a fixed total rms energy, dissipation is reduced if the energy of the higher frequency waves is comparable to the lower frequency ones (flatter spectra) with respect to the case in which most of the energy is contained in the low frequency modes (steeper spectra) (Verdini et al. 2005).

The eqs. 2 can be simplified including the systematic variation of the Elsässer amplitude in a new normalized variable $\mathbf{z}_N^\pm = \mathbf{z}_O^\pm(M_a \pm 1) / \sqrt{M_a}$, which reduces to $\mathbf{z}_N^\pm = \pm \mathbf{z}_O^\pm \rho^{1/4}$ in the limit of small alfvénic mach number $M_a = U/V_a \rightarrow 0$ (cfr. Heinemann & Olbert 1980).

After Fourier transforming in time the linear equations and adding the phenomenological nonlinear term one obtains,

$$(U \pm V_a) \mathbf{z}'_N \mp i\omega \mathbf{z}_N^\pm - \frac{1}{2}(U \pm V_a) \frac{V'_a}{V_a} \mathbf{z}_N^\mp = -\frac{|Z_O^\mp|}{L} \mathbf{z}_N^\pm \quad (3)$$

(the prime indicates a derivative with respect to r). The numerically integrated equations are:

$$\mathbf{z}'_N \mp i \frac{\omega}{U \pm V_a} \mathbf{z}_N^\pm - \frac{1}{2} \frac{V'_a}{V_a} \mathbf{z}_N^\mp = -\frac{|Z_O^\mp|}{(U \pm V_a)L} \mathbf{z}_N^\pm \quad (4)$$

for the corona, while for the photosphere and the chromosphere one gets:

$$\mathbf{z}'_N \mp i \frac{\omega}{V_a} \mathbf{z}_N^\pm + \frac{1}{2} \frac{V'_a}{V_a} \mathbf{z}_N^\mp = \mp \frac{|Z_O^\mp|}{V_a L} \mathbf{z}_N^\pm \quad (5)$$

The second, third and last coefficient in eqs. 4-5 represent the propagation (P), reflection (R) and nonlinear dissipation (NL) coefficients respectively (inverse of parallel wavelength, reflection scale height, nonlinear length scale). The dissipative feature of the nonlinear terms can be shown multiplying the above eq. 3, in its old variables form, by the complex conjugate $\mathbf{z}^{\pm*}$ to obtain the evolution equations for the Elsässer energies at a given frequency $E^\pm \equiv \frac{1}{2} |\mathbf{z}^\pm(\omega)|^2$. On the RHS one gets $-|\mathbf{z}^\pm|^2 |Z^\mp|/L$, which is independent of the phase difference between the two fields and involves the total amplitude of the fluctuations (the same term appears in the equation for a static atmosphere). In the presence of a wind, energy flux as conserved quantity is replaced, for linearly propagating waves, by the total wave action flux, which may be written as the difference between an outgoing and ingoing flux:

$$S^* = S^+ - S^- = \frac{1}{4} \rho U A \left[\frac{U + V_a}{U V_a} (\mathbf{U} + \mathbf{V}_a) |\mathbf{z}^+|^2 - \frac{U - V_a}{U V_a} (\mathbf{U} - \mathbf{V}_a) |\mathbf{z}^-|^2 \right] \quad (6)$$

(+, – refer to outward/ingward direction and S is the wave action).

The inward wave action density vanishes at the Alfvén critical point ($X_a \approx 13 R_\odot$, where the Alfvén speed equals the wind speed), so one may write $S^* = S_0^+ - S_0^- = S_c^+$, where the index c stands for the critical point, while the index 0 refers to the base of the layer. Amplitude and the phase of the outward propagating Elsässer field (\mathbf{z}^+) at X_a define the natural boundary conditions, since the critical point is a regular singular point for the incoming wave equation, because phase velocity of the mode vanishes there: total wave action density is imposed and the amplitude and phase of \mathbf{z}^- can be derived demanding the regularity of the solutions at X_a . However, boundary conditions are chosen to assure an amplitude of the rms velocity field fluctuations (i.e. summed over the whole spectrum)

of $\approx 40 \text{ km s}^{-1}$ at $1 R_{\odot}$, as constrained by observations (Banerjee et al. 1998), with an assigned spectral distribution: this requires some trial and error since nonlinearity does not allow rescaling of the photospheric amplitude by simply rescaling values at the critical point X_a . The shape of photospheric spectrum is imposed approximately thanks to the quasi-linear properties of the waves in the photosphere-chromosphere layer (small wave amplitudes) and the fact that transmission and nonlinearity yield frequency-independent evolution in the low corona, as shown in the next section. Given a slope p at the Alfvénic critical point, the transmission coefficient of the static layer $T(\omega)$ (see Krogulec & Musielak 1998 for discussion on it),

$$T(\omega) = \frac{S_c^+}{S_0^+} = \frac{\rho_c V_{ac}}{\rho_0 V_{a0}} \frac{|\mathbf{z}_c^+|^2}{|\mathbf{z}_0^+|^2} = \frac{|\mathbf{z}_{Nc}^+|^2}{|\mathbf{z}_{N0}^+|^2} \quad (7)$$

can therefore be used to correct the initial spectrum $|\mathbf{z}^+(\omega)| = |\mathbf{z}^+(\omega_0)| \times (\omega/\omega_0)^p$ to the desired spectrum at the photosphere imposing $|\mathbf{z}^+(\omega)| = |\mathbf{z}^+(\omega_0)| \sqrt{T(\omega)} \times (\omega/\omega_0)^p$. In order to describe the spectrum 32 modes are chosen in the range of frequency between 10^{-6} Hz and 10^{-2} Hz with increasing resolution at higher frequencies.

The phenomenological turbulent length scale varies as $L(r) = L_0 \times \sqrt{A(r)}$, where $L_0 = 34,000 \text{ km}$ is imposed at the coronal base and corresponds to the average size of the supergranules. The waves are propagated from the Alfvénic critical point forward (to the Earth orbit) and backward (till the base of the corona) by integration of eqs. 4. The conservation of the energy flux across the transition region allows one to determine the Elsässer fields below the discontinuity which are propagated back to the base of the photosphere using eqs. 5.

3. RESULTS

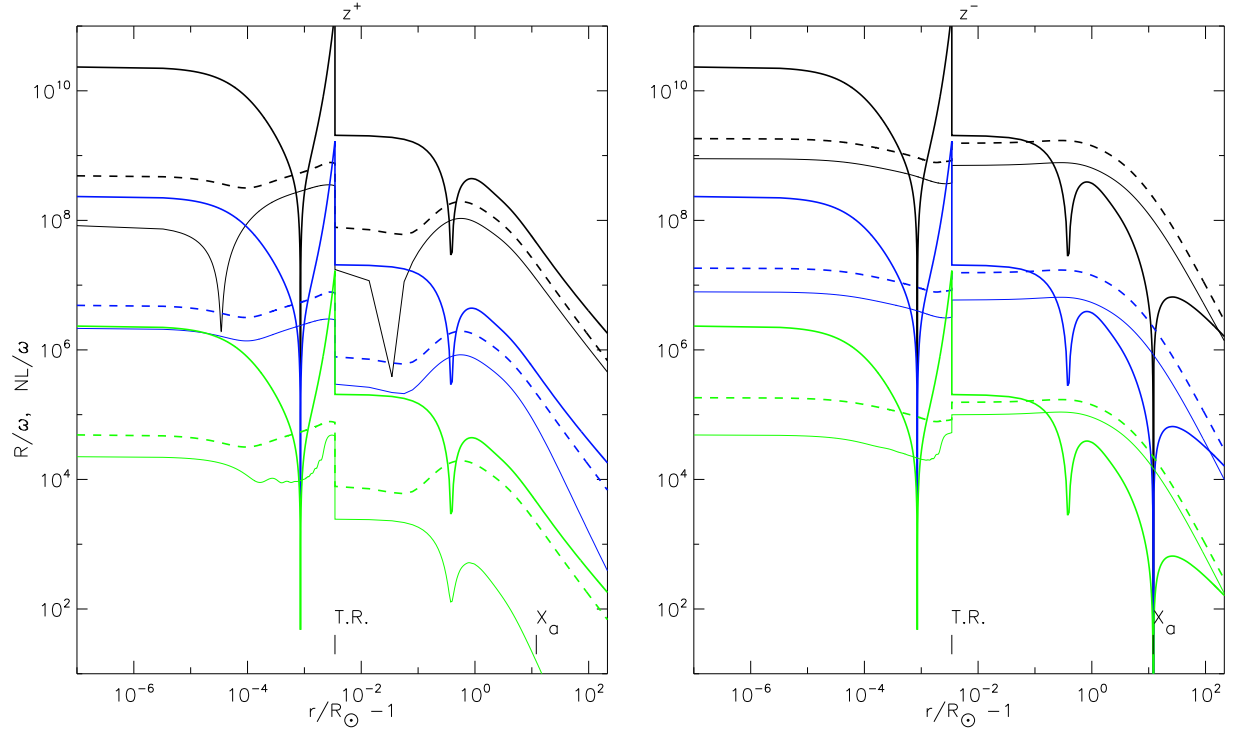


Fig. 2.— Comparison of the reflection (R, thick solid line) and nonlinear coefficient (NL, thick dashed line) normalized to the propagation coefficient (P) for the outgoing and ingoing wave at three different frequencies (10^{-6} Hz, 10^{-4} Hz, 10^{-2} Hz; black, blue and green lines respectively). Also shown in thin solid line is the contribution of each frequency wave to the nonlinear coefficient. The photospheric frequency spectrum is flat and the boundary conditions at X_a are set to get a rms velocity field fluctuation at the coronal base $\delta u = 40 \text{ km s}^{-1}$.

Following Velli 1993 we compare the characteristic lengthscales of eqs. 4-5 in the two layers. First consider the thick lines in fig. 2 which represent the reflection and nonlinear coefficients (solid and dashed line respectively) normalized to the propagation coefficient for $\omega = 10^{-6}$ Hz, 10^{-4} Hz, 10^{-2} Hz (black, blue and green lines respectively) for a flat photospheric spectrum. Reflection has a maximum at the transition region and it falls off by a factor of about 100 in the corona (because of the density drop). The zeros in the reflection coefficient appearing for both the z^+ and the z^- depend on the fact that $V_a' = 0$ (approximately in the corona), while the one located at X_a appears only for the backward propagating waves since the propagation coefficient becomes infinite there (see eq. 4). For the outward propagating wave (left panel) reflection is generally much greater (a factor 100) than dissipation in the photosphere-chromosphere and in the very low corona (below $\approx 1.2R_\odot$). Further out the nonlinear dissipation is smaller than reflection but of the same order of magnitude. For the inward propagating wave (right panel), again reflection dominates in the photosphere-chromosphere (by a factor of 10), but in the corona the dissipative coefficient is comparable or much greater than the reflection coefficient.

The *relative* dissipation of the linearly conserved quantities, as defined below in eq. 8, has hence different features in the two layers. In fig. 3 we plot the total wave action density for the corona (main panel) and the total wave energy flux for the static layer (sub panel) normalized to their base value for all the frequencies which form the spectrum, i.e.

$$\frac{S^*(r, \omega)}{S_0^*(\omega)} = \frac{|\mathbf{z}_N^+|^2 - |\mathbf{z}_N^-|^2}{|\mathbf{z}_{N_0}^+|^2 - |\mathbf{z}_{N_0}^-|^2} = 1 - \frac{1}{2(|\mathbf{z}_{N_0}^+|^2 - |\mathbf{z}_{N_0}^-|^2)} \int_{r_0}^r \frac{dr}{LV_a} \left(\frac{|Z_O^-|}{1 + M_a} |\mathbf{z}_N^+|^2 + \frac{|Z_O^+|}{1 - M_a} |\mathbf{z}_N^-|^2 \right), \quad (8)$$

with the normalization used to derive eqs. 3: the coefficients appearing in the integral are the nonlinear frequency integrated coefficients discussed above.

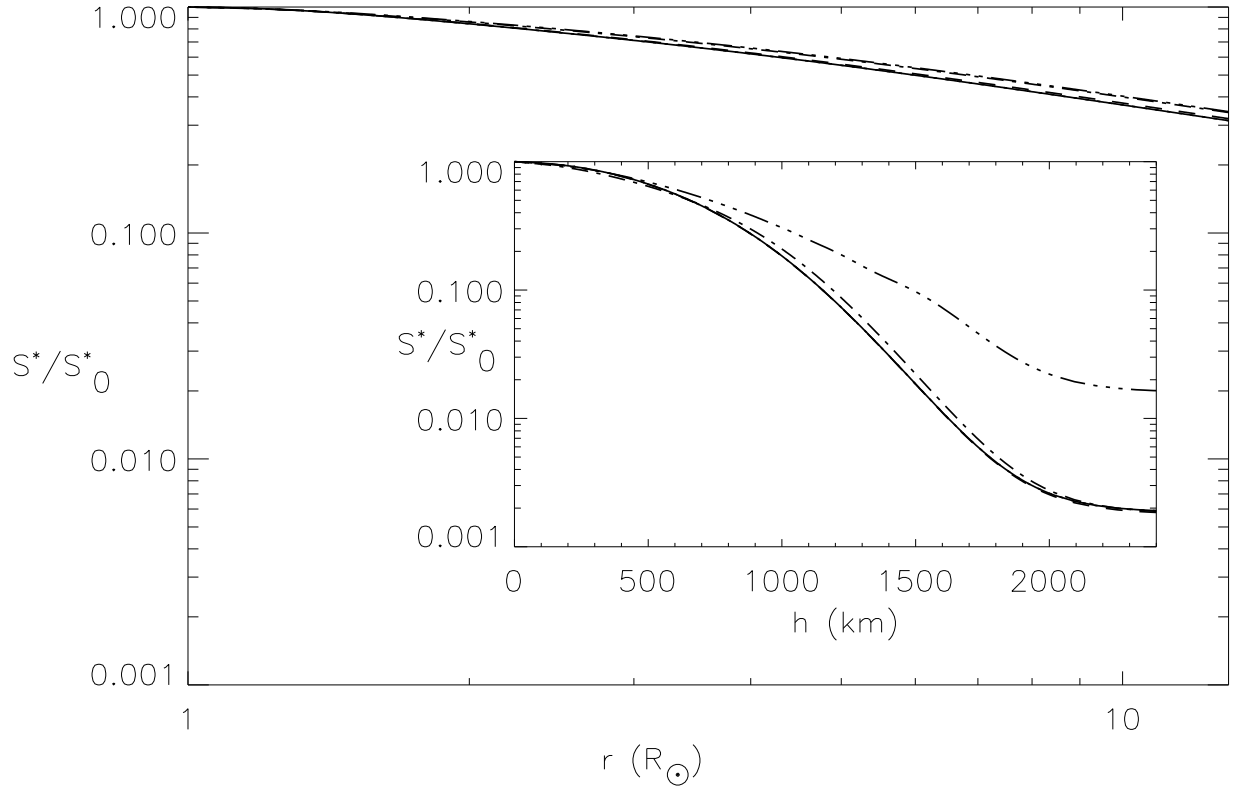


Fig. 3.— Normalized wave action density for the corona as function of distance for 5 frequencies (10^{-6} Hz solid line, 10^{-5} Hz dotted line, 10^{-4} Hz dashed line, 10^{-3} Hz dotted-dashed line, 10^{-2} Hz triple-dotted-dashed line). The wave energy flux for the photosphere-chromosphere is plotted in the subpanel with the same line coding.

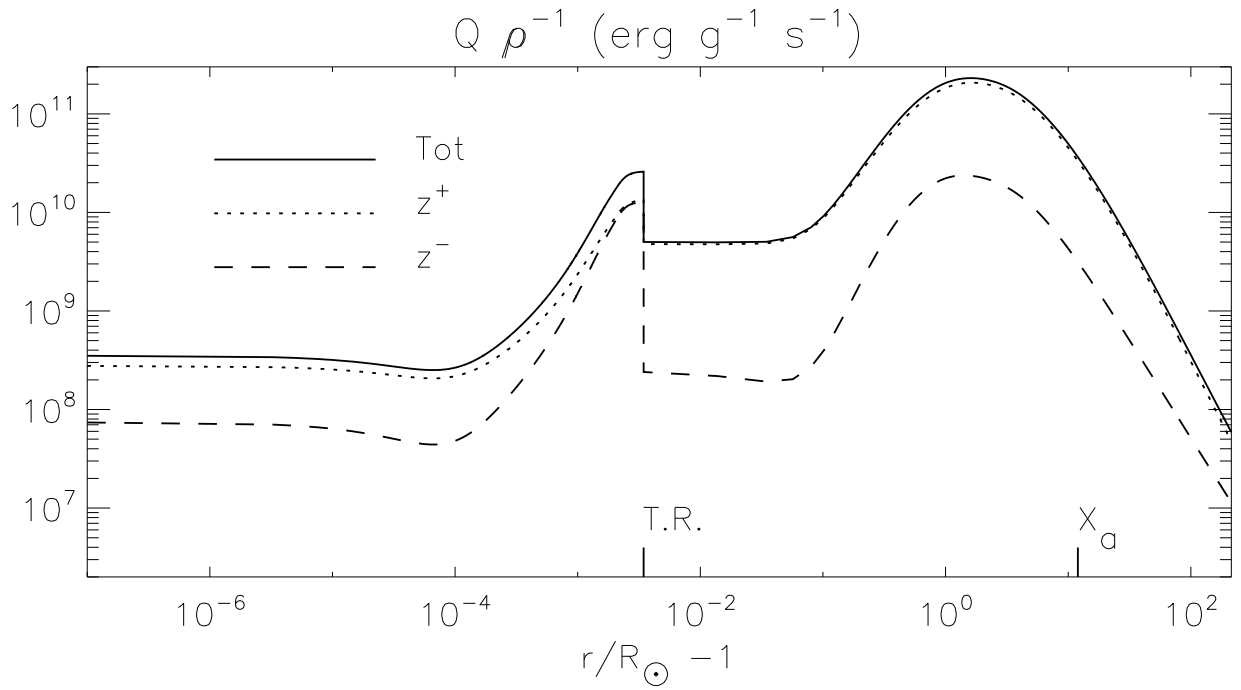


Fig. 4.— Heating rate per unit mass integrated over the whole spectrum as function of heliocentric distance. The contribution of the ingoing (dashed line) and outgoing (dotted line) heating rate is also shown. The transition region (T.R.) and the Alfvénic critical point ($X_a \approx 13 R_{\odot}$) are indicated on the x axis.

In the upper chromosphere the flux tube expansion is very rapid and reflection is strong, both the ingoing and outgoing wave contribute to the damping of the energy flux (comparable -less than one order of magnitude difference- nonlinear coefficient and wave amplitudes) and the relative dissipation is very high. Low frequency modes (lower plot in the subfigure) are the most damped (the most reflected) while high frequency modes (higher plots) are the less damped. In fact, inspection of eq. 8 reveals that the relative dissipation is quadratic in the frequency dependent wave amplitudes ($|\mathbf{z}_N^\pm|^2$) which in turn increase with decreasing frequency because of the different reflection rate. In the corona, instead, beyond $2R_\odot$ the dissipation coefficient for the outgoing waves is weaker and their amplitudes grow, reflection is weaker as well, and an imbalance between outgoing and ingoing fluxes holds. Only the former contribute to the wave action density dissipation since now the dominant quadratic dependence in eq. 8 comes from the outgoing mode (see for example the approximate conservation form used by Cranmer & van Ballegoijen 2005). Note that for all frequencies the wave action density decreases at approximately the same rate. It turns out that the amplitude evolution is driven mainly by the nonlinear, frequency independent, term in the corona and by the reflection, frequency dependent, term in the photosphere-chromosphere, a feature we will find again studying the power spectrum evolution.

In comparison the heating rate per unit mass, an *absolute* measure of energy dissipation, integrated over the spectrum,

$$\frac{Q}{\rho} = \frac{Q^+}{\rho} + \frac{Q^-}{\rho} = \frac{|Z^+|^2|Z^-| + |Z^-|^2|Z^+|}{L(r)}, \quad (9)$$

is generally higher in the corona than in the photosphere-chromosphere, as shown in fig. 4. In the latter layer both the ingoing and outgoing wave contributes to the total amount of heating rate, while in the former most of the dissipation comes from the outgoing mode. The absolute dissipation is quadratic in the frequency integrated wave amplitudes and in the corona outgoing wave are allowed to grow almost undamped (low relative dissipation) but the existence of a small seed of ingoing wave assures a large absolute dissipation. This is not true in the photosphere-chromosphere, before the rapid expansion of the flux tube, where the wave amplitude is small and there is a small imbalance between outgoing and ingoing propagating wave amplitudes.

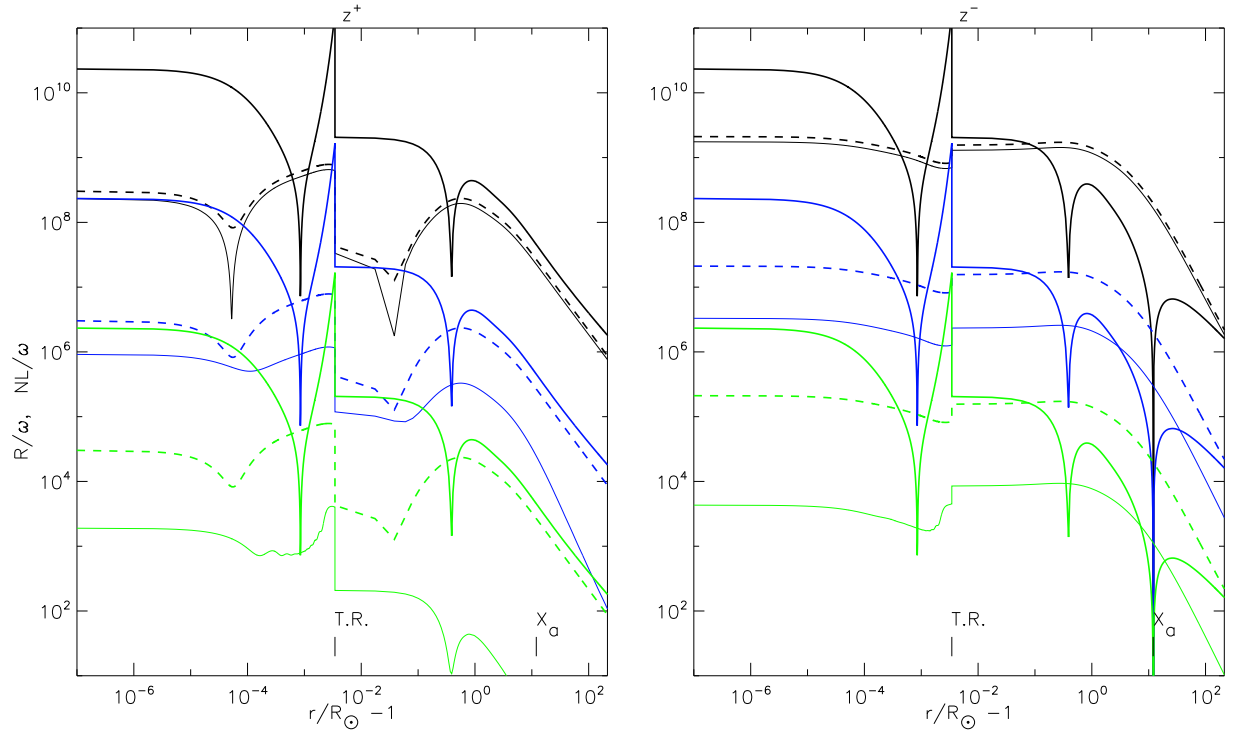


Fig. 5.— Same as fig. 2 for a photospheric Kolmogorov-like frequency spectrum

The effect of a different slope of the initial spectrum can be understood analyzing the contribution of each frequency to the nonlinear coefficient, plotted in thin lines in fig. 2. Starting with a flat photospheric frequency spectrum results in an approximately equal contribution to the total nonlinear term in the whole atmosphere, except for the outer corona where the nonlinear coefficient for the outward propagating wave is made up of essentially backward propagating waves at low frequencies. Note also that the frequency decomposed nonlinear coefficient is approximately the same for outgoing and ingoing propagating waves in the photosphere-chromosphere since reflection is high enough compared to dissipation. It follows that if a Kolmogorov-like photospheric spectrum ($E/\omega \propto \omega^{-5/3}$) is imposed, the nonlinear term is mainly made up of low frequency waves for both counterpropagating waves, in both the layers. This can be seen in fig. 5 comparing the dashed thick lines and the solid thin lines: for $\omega \gtrsim 10^{-4}$ Hz the contribution to the nonlinear coefficient is generally less than 10%. An exception is found below $2R_{\odot}$ for the outgoing mode, since reflection is high even for intermediate frequency wave (see fig. 7 for the photospheric layer). Note that a deep in the (frequency integrated) nonlinear coefficient for the outgoing mode appears below the location of vanishing reflection in both the photosphere and low corona, since the energy resides mainly in the low frequency mode.

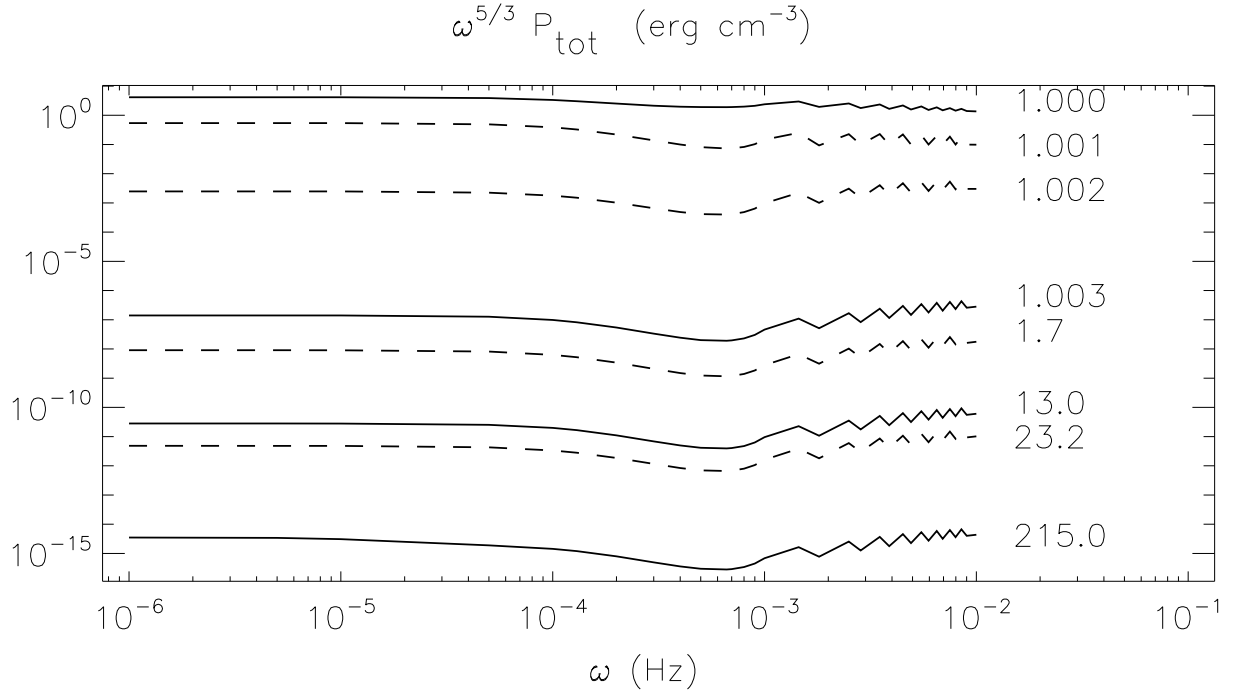


Fig. 6.— Compensated power spectrum as function of heliocentric distance for a photospheric kolmogorv-like initial spectrum. Each curve is labelled with the corresponding heliocentric distance in unit of R_{\odot} . From top to bottom, solid lines indicate the photospheric base, the T.R., X_a and 1 AU.

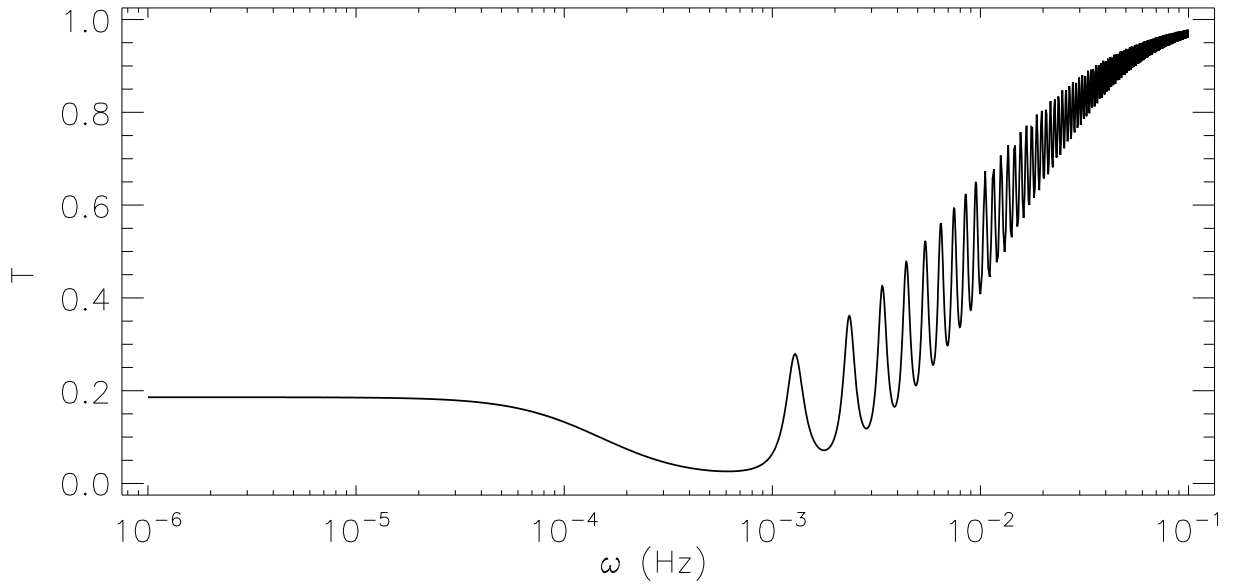


Fig. 7.— Transmission coefficient for the photosphere-chromosphere as function of frequency.

This separate behavior in the two layers has strong consequences on spectral evolution. In fig. 6 the (compensated) total power in the fluctuations is plotted for different heliocentric distances. An almost Kolmogorow-like spectrum is imposed at the base of the photosphere with a procedure described at the end of section 2. At very low frequencies the spectrum practically does not evolve, in the whole domain, while there is a tendency to steepen at low-intermediate frequencies (10^{-5} Hz $\lesssim \omega \lesssim 10^{-3}$ Hz). The behavior at high frequencies is quite complicated. Some irregularities appear very close to the base of the photosphere and the overall tendency is that of flattening. Note, however, that most of the changes in the shape occur in the photosphere-chromosphere where the waves display a strong frequency dependent behavior. This makes the spectral evolution very similar to the linear case, below the transition region (except the energy level of the spectrum), and the appearance of the irregularities can be interpreted by means of the linear analysis. Accordingly, in fig. 7 we plot the transmission coefficient, defined in eq. 7, as function of frequency for the photosphere-chromosphere. Note that the transmission is constant at low frequency, decreases at intermediate frequencies and increase again at high frequencies, where several transmission peaks appear: basically all spectral evolution is qualitatively reproduced. The peaks originate from the discontinuity in the reflection scale height at the transition region (Velli 1993). In fact the amplitude of the reflected waves shows some nodes inside the domain and when their location coincides with the base of the photosphere the transmission is enhanced (a condition which depends on the frequency of the waves, see Hollweg 1978). When nonlinearities are introduced the location of the nodes depends also on the wave amplitude imposed at X_a (see Verdini et al. 2005) and similarly if these nodes are located near the base of the photosphere the irregularities in the spectrum appear.

The slope of the spectrum imposed at the photosphere has negligible effects on the total power spectral evolution, however it changes the amount of energy residing in the ingoing and outgoing mode (or in the kinetic or magnetic fluctuations) at large distances and some constraints on the slope can be obtained using the available observational data. In fig. 8 the Elsässer energies E^\pm integrated over the frequency spectrum are plotted (solid and dashed line respectively) along with the Ulysses and Helios data (Bavassano et al. 2000b), for a Kolmogorov (thick lines) and a flat (thin lines) initial slope with $\delta u = 40$ km s $^{-1}$ at the coronal base. Both the data and the expected slopes are reproduced by the Kolmogorov-like photospheric spectrum while the flat one has too high outgoing energy and too low ingoing energy. The effect of high energy at high frequency waves is that of dissipating the inward wave, since they are mainly outward propagating: as a result outgoing waves are allowed to propagate almost undamped and their energy content is hence higher. Note that in the Kolmogorov case a deep, very close to the coronal base, appears as a signature of vanishing

ingoing waves, a feature of the low frequency reflected waves. This results in a vanishing absolute dissipation (heating) which is not found for the flat case and has important consequences for the acceleration and heating of the solar wind.

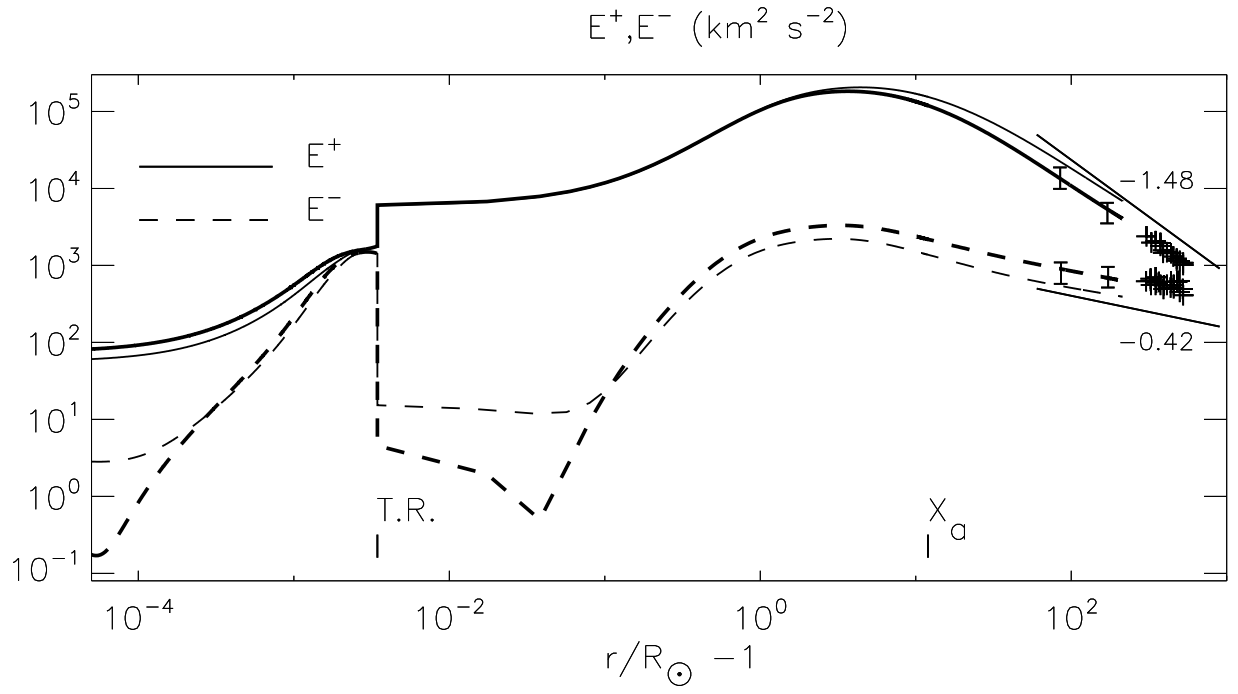


Fig. 8.— Frequency integrated Elsässer energies as function of heliocentric distance for a photospheric Kolmogorov spectrum with $\delta u = 40 \text{ km s}^{-1}$ at the coronal base. Symbols indicate observational constraints (see text for explanation).

In the following we consider only a Kolmogorov spectrum. In fig. 9 the root mean square amplitude of velocity field fluctuation integrated over the whole spectrum is plotted as function of heliocentric distance (solid line, in dotted line we plot also the magnetic field fluctuation in velocity unit) along with some observational data (taken from Cranmer & van Ballegoijen 2005, to which we address for comment on the data set):

- Filled diamonds are nonthermal line broadening velocities measured by SUMER on the disk (Wilhelm et al. 1995),
- Crosses are nonthermal velocities derived from SUMER observations above the solar limb (Banerjee et al. 1998)
- The box represents the upper and lower limit given by Esser et al. 1999 from UVCS off-limb data
- Stars are early measurements from Armstrong & Woo 1981
- The bars are recent measurements of transverse velocity field fluctuation using radio scintillation (Canals et al. 2002)
- Filled bars are the Helios and Ulysses data for the Elsässer energies, from Bavassano et al. 2000b, rewritten in term of the velocity field fluctuation assuming equipartition between magnetic and kinetic energy.

Note that the Helios and Ulysses data are obtained averaging over periods $\gtrsim 1$ hour (corresponding to $\omega \lesssim 10^{-4}$ Hz) while all the other points in the figure refers to rms values.

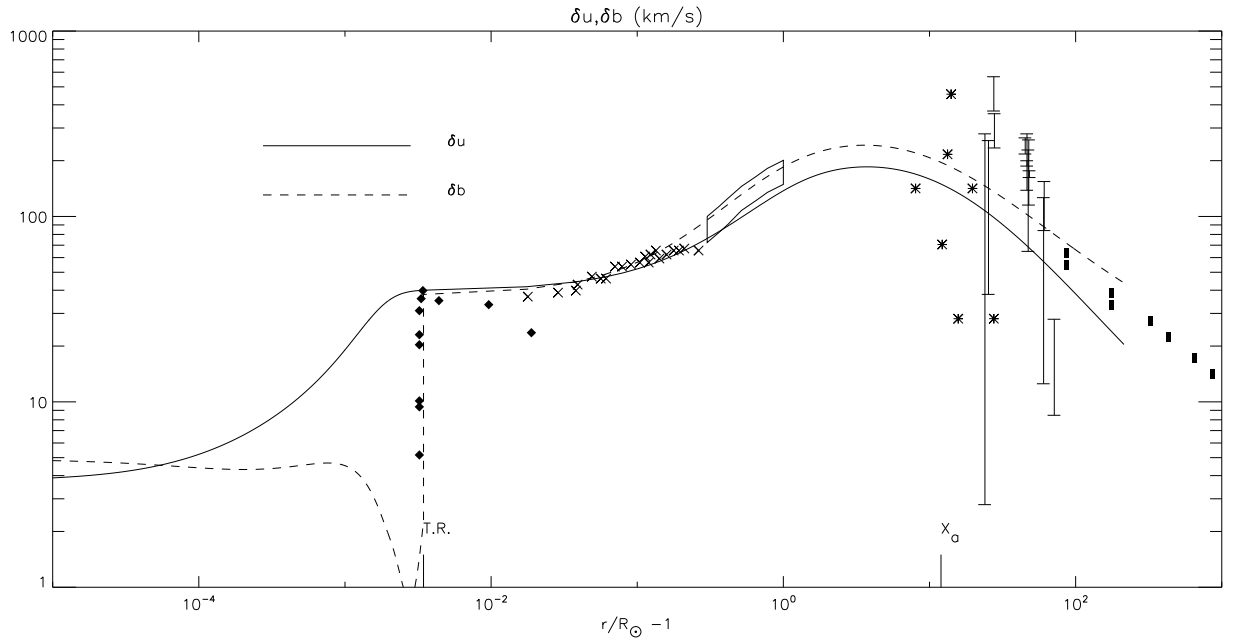


Fig. 9.— Root mean square amplitude δu and δb (in velocity units) as function of heliocentric distance for a photospheric Kolmogorov spectrum with $\delta u = 40 \text{ km s}^{-1}$ at the coronal base. Symbols indicates observational constraints (see text for explanation).

The overall agreement is quite good, even if data suggest a smaller power (more dissipation) just above the T.R. and more power (less dissipation) at about $2R_{\odot}$. Note that because of the equipartition assumption the Helios and Ulysses data disagree with the integrated quantities (the correct comparison has already been made above in fig. 8). As noted by Cranmer & van Ballegoijen 2005 the longitudinal velocity fluctuation data (filled diamonds) agree very well with the magnetic field fluctuation amplitudes (dashed line) and could indicate wave coupling among transverse and longitudinal mode. At leading order compressive effects are driven by the magnetic pressure originating from the incompressible fluctuations and represent a way for Alfvén waves to get rid of the energy excess above the T.R.. If these compressional waves are isotropic and suffer some dumping via shock formation, or other processes active in the low corona, they can reproduce the measured parallel δu and supply the heating needed by current model of wind acceleration.

4. CONCLUSIONS

In this paper we have modeled the nonlinear evolution of Alfvén waves propagating through the photosphere, the corona and the solar wind till 1 AU. Nonlinear interactions occur between outward propagating and reflected waves, and it is assumed that a nonlinear cascade develops preferentially in a direction perpendicular to that of propagation, which we take to coincide with the direction of the mean radial magnetic field.

While the phenomenological nonlinear term acts as a dissipative sink for both outward and inward waves, independently of the wave frequency, reflection, provided by the stratification of the layer, is generally strong at low frequencies and decreases with increasing frequency.

We find that most of the heating occurs in the low corona (below the Alfvénic critical point), while very little power is dissipated below the transition region. For reasonable velocity field fluctuations at the base of the photosphere a sufficient amount of energy flux is transmitted through the transition region. The adopted frequency coupling is not able to reproduce the observed spectral slope and evolution in the Alfvénic range even though frequency integrated data at large distances constrain the outer spectrum to be steep (-5/3 slope). The modification of the frequency spectrum occurs mainly in the chromosphere and in the photosphere since waves experience a strong reflection at all the frequencies considered, while in the corona and the solar wind the spectrum maintains approximately the same shape one finds at the coronal base.

Nonlinear dissipation based on reflection acts in different ways depending both on the (ingoing and outgoing) wave amplitude and on the layer considered. In the corona, reflection is not very high but the outgoing wave amplitude is allowed to grow, so that the wave evolution is driven by the nonlinear interactions (all the modes evolve in the same way) and one finds a strong heating rate in the Sub-Alfvénic corona.

In the photosphere-chromosphere a strong reflection rate, combined with small wave amplitudes, leads to an evolution similar to the linear case, which depends on frequency, and a small heating rate.

As a result most of the wave energy dissipation takes place in the first 4 solar radii above the coronal base. The driving modes for dissipation are the modes which experience the biggest reflection, generally low frequency modes. However depending on the model of atmosphere, i.e. on its characteristic scale height, and on the energy distribution, i.e. flat or steep spectra, intermediate frequency modes can be important as well.

The spectral shape varies mainly below the transition region, it steepens at low-intermediate frequencies (10^{-5} Hz $\lesssim \omega \lesssim 10^{-3}$ Hz) and flattens at high frequencies ($\omega \gtrsim 10^{-3}$ Hz) showing the characteristic features (energy peaks and frequency distribution) one finds in the transmission coefficient (linear behavior). In the corona instead, it maintains approximately the shape one finds beyond the T.R., because of the form of the nonlinear term adopted. The very low frequency range ($\omega \lesssim 10^{-5}$ Hz) practically does not evolve in the whole layer and it keeps the original slope at the photosphere. With this model of nonlinearities one can conclude that the spectrum one finds at 1 AU is basically the same spectrum at the base of the corona.

The input spectrum at the photosphere, whatever the shape is, is instead strongly modified by the transmission properties of the atmosphere below the transition region (independently of the model used for the nonlinear interaction). The energy peaks in the spectrum, resulting from an enhanced transmission at high frequencies, indicate that, even in presence of nonlinear interactions, the photospheric layer act as a filter for the energy injected through photospheric footpoint motion, if a smoothing of the forcing frequency is to be present, it must occur in this highly stratified layer.

The data at large distances suggest that energy at high frequency should be very low, however we find an energy increase at high frequency. Since the spectral evolution in corona depends also on the approximate frequency coupling contained in the nonlinear term, constraints on the photospheric input spectrum can not be given safely. Given that high frequency waves are transmitted through the T.R. and are quite energetic in the very low corona some other mechanism must be invoked to dissipate high frequency waves or a better modeling of the nonlinearities, which we plan to do in future works.

As first pointed out by Hollweg 1981, such high frequency energy reservoir can be the source for plasma heating processes operating in the low corona. Note that not only the peaks contribute to the energy budget, but the general flattening of the spectrum is important as well.

A comparison with measurements of δu suggests that the model can be considered a very good approximation in the outer corona and solar wind while, despite the good agreement found in the low corona, some other processes must be invoked to reproduced the observed features below the alfvénic critical point, such as compressible effects and wave coupling, especially in the chromosphere and photosphere. Other models of turbulent transport have been constructed to fit the decay of turbulence with distance from the sun in the solar wind beyond 1 AU (Smith et al. 2001; Breech et al. 2005) as well as to explain the extended heating in this region. Here the Alfvén speed can be neglected in the transport of the fluctuations, so that in some sense our model equations should be consistent with theirs, when rewritten in terms of the second order moments. A generalisation of turbulence transport equations, consistent both in the corona, acceleration region and solar wind is a topic of current research.

We would like to thank the IPAM program “Grand Challenge Problems in Computational Astrophysics” at UCLA where this work was completed. We also thank S. Oughton and W. H. Matthaeus for useful discussion.

REFERENCES

- Armstrong, J. W. & Woo, R. 1981, *Astron. Astrophys.*, **103**, 415
- Banerjee, D., Teriaca, L., Doyle, J. G., & Wilhelm, K. 1998, *Astron. Astrophys.*, **339**, 208
- Bavassano, B., Pietropaolo, E., & Bruno, R. 2000a, *J. Geophys. Res.*, **105**, 12697
- Bavassano, B., Pietropaolo, E., & Bruno, R. 2000b, *J. Geophys. Res.*, **105**, 15959
- Breech, B., Matthaeus, W. H., Minnie, J., et al. 2005, *Geophys. Rev. Lett.*, **32**, 6103
- Canals, A., Breen, A. R., Ofman, L., Moran, P. J., & Fallows, R. A. 2002, *Annales Geophysicae*, **20**, 1265
- Casalbuoni, S., Del Zanna, L., Habbal, S. R., & Velli, M. 1999, *J. Geophys. Res.*, **104**, 9947
- Cranmer, S. R. & van Ballegoijen, A. A. 2005, *ApJS*, **156**, 265

- Del Zanna, L., Velli, M., & Londrillo, P. 2001, *Astron. Astrophys.*, **367**, 705
- Dmitruk, P. & Matthaeus, W. H. 2003, *Astrophys. J.*, **597**, 1097
- Dmitruk, P., Matthaeus, W. H., & Lanzerotti, L. J. 2004, *Geophys. Rev. Lett.*, **31**, 21805
- Dmitruk, P., Matthaeus, W. H., Milano, L. J., & Oughton, S. 2001a, *Physics of Plasmas*, **8**, 2377
- Dmitruk, P., Matthaeus, W. H., Milano, L. J., et al. 2002, *Astrophys. J.*, **575**, 571
- Dmitruk, P., Milano, L. J., & Matthaeus, W. H. 2001b, *Astrophys. J.*, **548**, 482
- Esser, R., Fineschi, S., Dobrzycka, D., et al. 1999, *ApJL*, **510**, L63
- Habbal, S. R., Esser, R., Guhathakurta, M., & Fisher, R. R. 1995, *Geophys. Rev. Lett.*, **22**, 1465
- Heinemann, M. & Olbert, S. 1980, *J. Geophys. Res.*, **85**, 1311
- Hollweg, J. V. 1978, *Solar Phys.*, **56**, 305
- Hollweg, J. V. 1981, *Solar Phys.*, **70**, 25
- Hollweg, J. V., Jackson, S., & Galloway, D. 1982, *Solar Phys.*, **75**, 35
- Kopp, R. A. & Holzer, T. E. 1976, *Solar Phys.*, **49**, 43
- Krogulec, M. & Musielak, Z. E. 1998, *Acta Astronomica*, **48**, 77
- Leroy, B. 1980, *Astron. Astrophys.*, **91**, 136
- Li, X., Habbal, S., Hollweg, J. V., & Esser, R. 1999, *J. Geophys. Res.*, **104**, 2521
- Mangeney, A., Grappin, R., & Velli, M. 1991, *Advances in Solar System Magnetohydrodynamics* (Priest, E. R. and Hood, A. W.), 327
- Matthaeus, W. H., Montgomery, D. C., & Goldstein, M. L. 1983, *Physical Review Letters*, **51**, 1484
- Matthaeus, W. H., Smith, C. W., & Oughton, S. 1998, *J. Geophys. Res.*, **103**, 6495
- Matthaeus, W. H., Zank, G. P., Oughton, S., Mullan, D. J., & Dmitruk, P. 1999, *ApJL*, **523**, L93
- Matthaeus, W. H., Zhou, Y., Zank, G. P., & Oughton, S. 1994, *J. Geophys. Res.*, **99**, 23421

- Munro, R. H. & Jackson, B. V. 1977, *Astrophys. J.*, **213**, 874
- Oughton, S., Dmitruk, P., & Matthaeus, W. H. 2004, *Physics of Plasmas*, **11**, 2214
- Oughton, S., Matthaeus, W. H., Dmitruk, P., et al. 2001, *Astrophys. J.*, **551**, 565
- Pruneti, F. & Velli, M. 1997, in *ESA SP-404: Fifth SOHO Workshop: The Corona and Solar Wind Near Minimum Activity*, 623–+
- Similon, P. L. & Zargham, S. 1992, *Astrophys. J.*, **388**, 644
- Smith, C. W., Matthaeus, W. H., Zank, G. P., et al. 2001, *J. Geophys. Res.*, **106**, 8253
- Suzuki, T. K. & Inutsuka, S.-i. 2005, *ApJL*, **632**, L49
- Tu, C.-Y. 1988, *J. Geophys. Res.*, **93**, 7
- Tu, C.-Y., Pu, Z.-Y., & Wei, F.-S. 1984, *J. Geophys. Res.*, **89**, 9695
- Velli, M. 1993, *Astron. Astrophys.*, **270**, 304
- Velli, M., Grappin, R., & Mangeney, A. 1989, *Physical Review Letters*, **63**, 1807
- Velli, M., Grappin, R., & Mangeney, A. 1991, *Geophys. Astrophys. Fluid Dynamics*, **62**, 101
- Verdini, A., Velli, M., & Oughton, S. 2005, *Astron. Astrophys.*, **444**, 233
- Wilhelm, K., Curdt, W., Marsch, E., et al. 1995, *Solar Phys.*, **162**, 189
- Zank, G. P., Matthaeus, W. H., & Smith, C. W. 1996, *J. Geophys. Res.*, **101**, 17093
- Zhou, Y. & Matthaeus, W. H. 1989, *Geophys. Rev. Lett.*, **16**, 755
- Zhou, Y. & Matthaeus, W. H. 1990, *J. Geophys. Res.*, **95**, 10291